THE ASTROPHYSICAL JOURNAL, 416:118–129, 1993 October 10

UNIFIED MODEL FOR X-RAY– AND RADIO-SELECTED BL LACERTAE OBJECTS

A. CELOTTI,[1] L. MARASCHI,[2,3] G. GHISELLINI,[4] A. CACCIANIGA,[3,5] AND T. MACCACARO[5]
Received 1992 December 14; accepted 1993 April 15

ABSTRACT

The existence of two populations of BL Lac sources, characterized by different spectral properties and number densities, has been confirmed by the recently obtained complete samples of radio- and X-ray–selected sources. In the framework of relativistic jet models, the different properties of the two populations can be accounted for if the X-ray radiation is less beamed than the radio one. We propose that this can be due to a larger opening angle of the flow velocity in the inner, X-ray–emitting part of a jet of constant bulk Lorentz factor. With these assumptions we compute the expected luminosity functions (LFs) in the radio and X-ray bands for beamed objects deriving from the same parent population but observed at different angles. We apply this formalism to X-ray–selected and radio-selected BL Lac objects, assuming FR I radio galaxies as the parent population. From the available data we derive here the radio LFs of X-ray–selected BL Lac objects and the X-ray LFs of radio-selected BL Lac objects in order to allow a statistically meaningful comparison of the two samples in the same band. We find the average bulk Lorentz factor and the opening angles of the X-ray– and radio-emitting parts of the jet. We conclude that FR I radio galaxies and X-ray– and radio-selected BL Lac objects can be the same phenomenon observed at decreasing angle to the jet axis.

Subject headings: BL Lacertae objects: general — galaxies: jets — galaxies: luminosity function, mass function — X-rays: galaxies

1. INTRODUCTION

Unification schemes are an attempt to understand the "essence" of active galactic nuclei (AGNs), by trying to separate the basic physical phenomena occurring in AGNs from orientation effects (e.g., Urry, Maraschi, & Phinney 1991a). On the other hand, if anisotropic emission occurs in a class of sources there should exist other sources intrinsically identical but observed at different orientation and consequently showing different properties.

Many observations indicate that the emission of BL Lac objects is strongly affected by beaming associated with relativistic bulk motion of the radiating plasma. Indeed, since the first suggestion by Blandford & Rees (1978), an increasing number of observations have been interpreted in terms of relativistic beaming models, such as superluminal motion (e.g., Zensus 1989), high brightness temperature, fast variability, paucity of X-ray self-Compton radiation (e.g., Blandford 1987), one-sidedness of parsec-scale radio jets, and the larger Faraday rotation identifying the "far" side of the jet (Laing 1988; Garrington et al. 1988).

Several authors (e.g., Browne 1983; Wardle, Moore, & Angel 1984; Padovani & Urry 1990) proposed one of the most promising hypotheses on the parent population of BL Lac objects. According to this suggestion, BL Lac objects are low-power (FR I) radio galaxies, observed at small angles with the jet axis. Circumstantial evidence for this unification model includes the power and morphology of the extended (supposedly unbeamed) radio emission of BL Lac objects (Antonucci & Ulvestad 1985), the properties of their host galaxies (Ulrich 1989; Abraham, McHardy, & Crawford 1991), the estimate of the incident continuum in highly ionized filaments in some radio galaxies (e.g., Morganti et al. 1992), the orientation of the line of sight with respect to the beaming direction predicted by the beaming indicators mentioned above (e.g., Ghisellini et al. 1993), and the comparison of number density and luminosity functions (LFs) of the parent and beamed populations (see below).

Recently two complete samples of BL Lac objects have become available, one selected on the basis of radio flux (Stickel et al. 1991), the other on the basis of X-ray flux (Morris et al. 1991). These samples showed conclusively that the broad-band energy distributions of the groups differ systematically, the X-ray–selected objects showing considerably smaller radio and optical luminosities relative to their X-ray luminosity. Notably, the radio-selected objects have X-ray luminosities comparable to the X-ray–selected ones. The two classes of sources can therefore be distinguished on the basis of the radio to X-ray spectral index $\alpha_{RX} \equiv -\log [F(\nu_X)/F(\nu_R)]/\log (\nu_X/\nu_R)$ (where all quantities refer to the source frame; $\nu_R = 5$ GHz, $\nu_X = 2$ keV, $\alpha_R = 0$, and $\alpha_X = 1$ are assumed in the flux K-correction). In the following we will call radio-loud (RBL) the objects with a steep radio–X-ray spectral index $\alpha_{RX} > 0.7$, and radio-weak (XBL) the objects with $\alpha_{RX} < 0.7$. As mentioned above there is a close corresponence between this parameter and the *observational* band of selection.

Stickel et al. (1991) and Morris et al. (1991) have computed the luminosity functions of radio-selected and X-ray–selected objects in the respective selection bands. Therefore it is now possible to use the absolute space densities to test and constrain beaming models. In a recent series of papers, Urry & Padovani tested the hypothesis that BL Lac objects are low-luminosity radio galaxies (FR I galaxies) beamed at us. They considered separately and independently the X-ray and radio luminosity functions of the parent population (FR I galaxies)

[1] Institute of Astronomy, Madingley Road, CB3 0HA Cambridge, UK.
[2] Dipartimento di Fisica, Università di Genova, Italy.
[3] Dipartimento di Fisica, Università di Milano, Via Celoria 16, 20133 Milano, Italy.
[4] Osservatorio Astronomico di Torino, Strada Osservatorio 20, 10025 Pino Torinese, Italy.
[5] Osservatorio Astronomico di Brera, Via Brera 28, 20121 Milano, Italy.

and derived the parameters of the beaming model by comparing the predicted X-ray or radio luminosity functions of BL Lac objects with the observed ones (Padovani & Urry 1990; Urry, Padovani, & Stickel 1991c). They found that the scheme is successful if the X-ray–selected objects have a bulk Lorentz factor $\Gamma \simeq 3$–4, and the radio-selected ones have a power-law distribution of Γ, extending up to $\Gamma = 40$, with $\langle\Gamma\rangle = 7.4$.

These results may suggest the existence of two different classes of BL Lac objects, with different bulk Lorentz factors. It was, however, proposed early on that *the relative numbers and the different energy distributions of XBL and RBL* could be understood *at the same time*, if in the same object the X-ray emission is beamed in a larger cone than the radio emission (Maraschi et al. 1986). Observers within the X-ray angles Θ_X would see similar X-ray fluxes, but only observers within the radio angles Θ_R would see a strong, relativistically enhanced ratio flux. Consequently the ratio of the radio to the X-ray flux (measured by α_{RX}) would change with viewing angle Θ: $\Theta < \Theta_R$ would correspond to RBLs, $\Theta_R < \Theta < \Theta_X$ to XBLs.

Ghisellini & Maraschi (1989) discussed a model in which the flow velocity of the relativistic plasma increases (accelerates) with radial distance, so that relativistic beaming is mild in the inner, X-ray–emitting region of the jet, but strong in the outer, radio-emitting region. This model will be called the "accelerating jet" model. In order to explain the observed energy distributions, a smooth acceleration from $\Gamma \sim 1$ in the inner region to $\Gamma \sim 4$–5 in the outer parts was required, implying a physical acceleration mechanism operating on a relatively large scale, a factor 10^2–10^3 at least in distance from the core. Since the X-rays are not beamed, it is difficult in this model to explain the rapid and large-amplitude X-ray variability (see, e.g., Treves et al. 1989).

Here we explore an alternative picture, in which the velocity is constant but the collimation of the jet increases with distance, that is, the solid angle subtended by the velocity vectors of the outflow decreases from the inner, X-ray–emitting, region to the outer, radio-emitting region. Note that large-scale radio jets indeed appear to become more collimated with increasing distance (e.g., Begelman 1992). We will call this model the "wide jet" model.

In a preliminary paper (Maraschi, Celotti, & Ghisellini 1991) we showed that the LF predicted by the wide jet model are consistent with the assumption that BL Lac objects are FR I galaxies beamed at us in a similar way as discussed by Padovani and Urry for the "accelerating jet" model. In fact, from the "statistical" point of view the two models are substantially equivalent.

Here we present the "wide jet" model in detail giving the relevant formulae. In addition we focus on the *joint* constraints on the *radio and X-ray* luminosity functions provided by the radio fluxes of the X-ray–selected objects and the X-ray fluxes of the radio-selected ones. Using published data on these samples we derive here the radio luminosity function of the X-ray–selected BL Lac objects and the X-ray luminosity function of the radio-selected, which, together with the LFs originally derived by Stickel et al. (1991) and Morris et al. (1991), allow a comparison of the two samples in the *same* band. The *relative number of XBL and RBL of equal X-ray luminosity*, which is estimated here for the first time, fixes the ratio of solid angles in the radio and X-ray band. In the "accelerating jet" model this also fixes the ratio of Γ_X to Γ_R, while in the "wide jet" model the solid angle ratio is attributed to the different collimation of the jet flow.

In both cases X-ray–selected objects should on average be observed at angles greater than radio-selected ones. The sequence FR I radio galaxy-XBL-RBL should therefore correspond to a decreasing viewing angle, similarly to the unified scheme explored by Padovani & Urry (1992) in the radio band for FR II, steep radio spectrum and flat radio spectrum quasars.

The structure of the paper is as follows: In § 2 we present the wide jet model, computing the beamed luminosity as a function of the viewing angle for wide jets. We then derive the expected luminosity function of the beamed objects assuming a given "parent population." In § 3 we discuss the qualitative predictions of the wide jet model and compare these predictions to the distribution of different types of objects in the plane of the X-ray versus radio luminosities, $L_X - L_R$. In § 4 we use the published X-ray and radio fluxes to compute the luminosity functions of the X-ray– and radio-selected samples, in both the X-ray and radio bands. We then derive the constraints imposed by the above data on the model parameters and present and discuss our findings in § 5. In § 6 we summarize our results.

2. THE LUMINOSITY FUNCTION OF "WIDE" JET OBJECTS

Let us consider a collimated plasma flow with constant bulk Lorentz factor Γ, intrinsic luminosity ℓ (as viewed by an observer comoving with the flow), and observed luminosity L. The line of sight makes an angle Θ with the jet axis. The radiation emitted by each element of the plasma is therefore beamed in a cone of half-angle Θ_c, corresponding to $\sin\Theta_c = 1/\Gamma$, that is, $\cos\Theta_c = \beta$, where β_c is the bulk velocity. If the velocity vectors of the streamlines of the flow are parallel, the angular dependence of the observed luminosity $L(\Theta)$ is given by the usual relation $L(\Theta) = \delta^p(\Theta)\ell$, where $\delta = 1/[\Gamma(1 - \beta\cos\Theta)]$ is the Doppler factor. The exponent p is assumed hereafter to be $p = 3 + \alpha$, where α is the spectral index. Such a value is appropriate for amplification of monochromatic luminosity from a moving blob of plasma, if particle acceleration continuously occurs (other more complicated cases have been discussed by Lind & Blandford 1985).

If the flow velocities are spread in a cone of half-angle Θ_j larger than Θ_c (wide jet), the effects of relativistic beaming will be diluted. In § 2.1 we derive expressions for the observed flux at different angles, and in § 2.2 we compute the predicted LF, comparing it with the case of parallel velocity flow (Urry & Shafer 1984) in some limiting cases.

2.1. *The Luminosity Enhancement*

Consider a relativistic flow with fixed bulk Lorentz factor Γ but with velocity directions uniformly spread in a cone of semiaperture Θ_j, larger than the critical semiaperture angle for relativistic beaming Θ_c. In this case the relation between the intrinsic and the observed luminosity at an angle Θ with the jet axis is

$$L(\Theta) = \ell R(\Theta) \equiv \frac{\ell}{\Delta\Omega_j}\int_0^{\Theta_j}\sin\theta\, d\theta\int_0^{2\pi}\delta^p(\Theta,\theta,\phi)d\phi \quad (1)$$

with

$$\delta(\Theta,\theta,\phi) = \frac{1}{\Gamma[1 - \beta(\sin\Theta\sin\theta\cos\phi + \cos\Theta\cos\theta)]}, \quad (2)$$

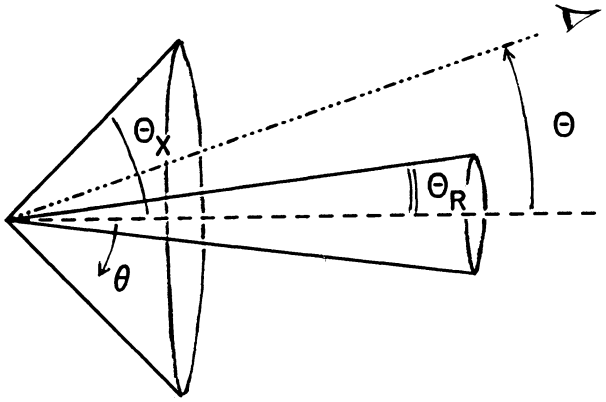

FIG. 1.—Schematic representation of the "wide" jet model. Θ_j is the jet opening angle, called Θ_X and Θ_R for the X-ray– and radio–emitting regions, respectively. Θ is the angle between the jet axis and the line of sight. ϕ is the azimuthal coordinate, and θ is the polar coordinate measured from the jet axis, which identify the position of a portion of the fluid.

where $R(\Theta)$ is the enhancement factor due to beaming, defined by equation (1), and the beaming factor $\delta(\Theta, \theta, \phi)$ is a function of the spherical coordinates θ and ϕ within the cone of half-angle Θ_j: ϕ is the azimuthal coordinate and the polar angle θ is measured from the jet axis (see Fig. 1). $R(\Theta)$ involves the integration of the contribution from each part of the jet flow: the integrand therefore depends on the angle, call it χ, between the line of sight and the velocity direction of each volume of the jet, the position of which is identified by the two angular coordinates θ and ϕ. The combination of sinusoidal functions multiplying β in equation (2) is just the cosine of χ. The solid angle subtended by the jet is $\Delta\Omega_j = 2\pi(1 - \cos\Theta_j)$.

For $\Theta = 0$, the integral in equation (1) simplifies in

$$L(0) = \ell \frac{2\pi}{\Delta\Omega_j} \frac{(1+\beta)^{p-1}}{\beta(p-1)} \times \Gamma^{p-2}\{1 - [\Gamma^2(1+\beta)(1-\beta\cos\Theta_j)]^{1-p}\} . \quad (3)$$

In general, equation (1) has to be calculated numerically, but for integer values of p there exist analytical solutions, which are derived in Appendix A.

Let us now derive $R(\Theta)$ in some simple limits with approximate but intuitive arguments.

First we estimate the observed luminosity at $\Theta < \Theta_j$. The behavior of $R(\Theta)$ can be understood considering that, for $\Theta < \Theta_j$, the radiation reaching the observer is mainly produced by plasma in a little cone of angle Θ_c around the line of sight. Since for $\Theta < \Theta_j$ there is always one of these little cones pointing at the observer, we expect $L(\Theta)$ to be approximately constant with a value approaching $L(0)$ (Fig. 2; see below).

Furthermore the number N of small cones of half-angle Θ_c within the Θ_j cone is simply the ratio of the subtended solid angles: $N = (1 - \cos\Theta_j)/(1 - \cos\Theta_c) \simeq (1+\beta)\Gamma^2(1 - \cos\Theta_j)$. Therefore

$$L(\Theta) \simeq \frac{\ell}{N}\delta^p(0) \simeq \frac{2\pi}{\Delta\Omega_j}\ell(1+\beta)^{p-1}\Gamma^{p-2}; \quad \Theta < \Theta_j , \quad (4)$$

where ℓ/N is the fraction of intrinsic luminosity emitted by the plasma in one small cone, and $\delta^p(0)$ is the enhancement factor at zero angle. In the limit of large Γ, equation (4) differs from the value given by equation (3) by the factor $(p - 1)$.

For a jet with opening angle $< 1/\Gamma$, (narrow jet, i.e., parallel velocities), one has $L(0) = \ell\delta^p(0) \sim (2\Gamma)^p\ell$, for $\Gamma \gg 1$. Equation (4) shows that the maximum observed luminosity from a wide jet is smaller than that of a narrow one by a factor $(1/N) \sim 1/[2\Gamma^2(1 - \cos\Theta_j)]$ which corresponds to the fraction of the jet beamed toward the observer.

By the same approximate arguments, we can derive the observed luminosity at $\Theta > \Theta_j$. In this case the main contribution to the observed flux comes from the plasma in the "$1/\Gamma$" little cone at an angle between $\Theta - \Theta_j$ and $\Theta - \Theta_j - 1/\Gamma$, on the border of the jet. Taking $\Theta - \Theta_j$ as the relevant angle we have

$$L(\Theta) \sim \frac{\ell}{N}\delta^p(\Theta - \Theta_j) = \frac{2\pi}{\Delta\Omega_j}\ell\frac{1}{(1+\beta)\Gamma^{p+2}[1 - \beta\cos(\Theta - \Theta_j)]^p} , \quad \Theta > \Theta_j . \quad (5)$$

The minimum luminosity corresponds to $\Theta = \pi/2$. At this value of Θ equation (5) has to be compared with $L(\pi/2) = \ell/\Gamma^p$ obtained in the case of parallel velocities. Depending on Θ_j and Γ, equation (5) can yield smaller or greater values than those obtained for parallel velocities.

In the previous calculations we have assumed that *all* the radiation is beamed. More generally, the observed luminosity $L(\Theta)$ can be the sum of two components: an unbeamed part, ℓ, due to stationary plasma, and a beamed one, $L_b(\Theta)$. Suppose further that the rest frame luminosity of the moving plasma is a fraction f of the unbeamed luminosity (Urry & Shafer 1984). In this case $L(\Theta) = \ell + L_b(\Theta) = \ell + f\ell R(\Theta) = \ell[1 + fR(\Theta)]$. Hereafter ℓ represents the total unbeamed luminosity, while the comoving luminosity in the beamed plasma, indicated as ℓ in equations (1)–(5), is given by $f\ell$. The enhancement factor $\bar{R}(\Theta)$ defined as

$$\bar{R}(\Theta) = 1 + fR(\Theta) \quad (6)$$

represents the ratio of the total observed luminosity to the unbeamed luminosity. Clearly the flux measured by an observer at angle Θ will be enhanced by the same factor. We also assume that f is independent of ℓ and constant for all sources.

Figure 2 shows the enhancement factor $\bar{R}(\Theta)$ versus Θ, for $\Gamma = 10$, $f = 1$, $p = 3$, and for different values of Θ_j. For comparison, in Figure 2 we also plot the amplification factor for the case of parallel velocities, $1 + f\delta^3(\Theta)$, for the same Γ. The spread of the velocity vectors produces a flat top in the enhancement factor: in fact for all angles smaller than Θ_j the amplification is almost constant, being dominated by the contribution of the small cone along the line of sight. In wider jets the number of such small cones is larger, and their fractional contribution is smaller: consequently, for $\Theta < \Theta_j$, $\bar{R}$ is inversely proportional to the jet angle.

2.2. *The Luminosity Function*

Given the relation between the intrinsic and observed luminosity for a single source (eqs. [1] and [6]), we can compute the luminosity function (LF) for the population of "beamed" objects $\Phi(L)$, from the luminosity function of the parent population $\Phi_u(\ell)$. This procedure was first developed by Urry & Shafer (1984). We define *beamed* an object whose viewing angle yields $L_b(\Theta) \geq \ell$. that is, $\bar{R} \geq 2$.

For a random distribution of jet directions in the sky, the probability $P(L, \ell)$ of observing a source with a given $L(\Theta)$ is

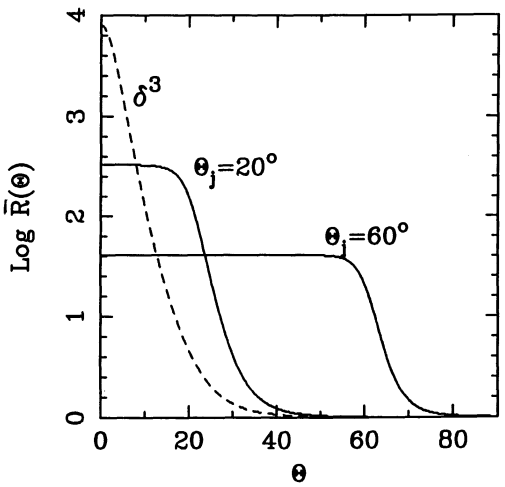

FIG. 2.—Intensity distribution as a function of the angle between the line of sight and the jet axis, represented by the enhancement factor $\bar{R}(\Theta)$ of the "wide" jet model. It is calculated for $\Gamma = 10$, $p = 3$, $f = 1$ and values of the semiaperture angle of the jet $\Theta_j = 20°$ and 60°. The dashed line represents $1 + f\delta^p$ for the same Γ.

distributed as the solid angle corresponding to that Θ, which for double-sided jets is

$$P(L, \ell)dL = \frac{d\Omega}{2\pi} = \sin\Theta\, d\Theta\,. \tag{7}$$

If the intrinsic luminosities have a distribution $\Phi_u(\ell)$ between $\ell_{\min}$ and $\ell_{\max}$, the observed luminosity function is

$$\Phi(L) = \int_{\ell_{\min}}^{\ell_{\max}} \Phi_u(\ell) P(L, \ell) d\ell\,. \tag{8}$$

Changing variable, from ℓ to Θ, and noting that

$$d\ell = -\frac{L}{\bar{R}^2(\Theta)} \frac{d\bar{R}(\Theta)}{d\Theta} d\Theta\,, \tag{9}$$

we obtain

$$\Phi(L) = -\int_{\Phi_1}^{\Theta_2} \Phi_u\left[\frac{L}{\bar{R}(\Theta)}\right] \frac{\sin\Theta}{\bar{R}(\Theta)} d\Theta \tag{10}$$

where Θ_1, Θ_2 are the limiting angles for which there are objects of observed luminosity L and intrinsic luminosity $\ell_{\min} < \ell < \ell_{\max}$. Θ_1 and Θ_2, which range between 0 and $\pi/2$, can be found by solving the equations

$$\begin{aligned} &L - \ell_{\max}\bar{R}(\bar{\Theta}_2) = 0 \quad \Theta_2 = \min(\bar{\Theta}_2, \pi/2) \\ &L - \ell_{\min}\bar{R}(\bar{\Theta}_1) = 0 \quad \Theta_1 = \max(\bar{\Theta}_1, 0)\,. \end{aligned} \tag{11}$$

The range of integration $[\Theta_1, \Theta_2]$ can be restricted to the opening angles of the jet, due to the definition of "beamed" population (see below).

Note that equation (10) is very general and can be used in all cases in which the emitted luminosity is anisotropic, once $\bar{R}(\Theta)$ is known. For instance, it can be used in the case of geometrically thin disks, where $L(\Theta) = L(0)\cos\Theta$, or in the case of thick disks (e.g., Urry, Marziani, & Calvani 1991b), where the presence of the funnel makes the emitted luminosity very anisotropic.

Due to the complexity of $\bar{R}(\Theta)$, the function $\Phi(L)$ has to be derived numerically. However, the approximate expressions for $L(\Theta)$ derived in § 2.1 can be used to have some insight about the general behavior of $\Phi(L)$.

Consider a parent population of objects with fixed luminosity ℓ. In the Urry & Shafer scheme, the probability of observing a luminosity L is $P(L, \ell) \propto L^{-(1+1/p)}$ in the entire allowed luminosity range. Here, instead, we must distinguish between viewing angles greater than the jet angle (corresponding to low observed luminosities), and smaller than the jet angle (corresponding to high luminosities).

In the former case $[L(\Theta > \Theta_j)]$, we have, from equation (5),

$$\frac{dL}{d(\Theta - \Theta_j)} = p\beta\Gamma\delta^{p+1}(\Theta - \Theta_j)\frac{\ell}{N}\sin(\Theta - \Theta_j); \quad \Theta > \Theta_j\,. \tag{12}$$

Then, using equations (5) and (7), we have

$$P(L, \ell) = \frac{1}{p\Gamma\beta}\left(\frac{\ell}{N}\right)^{1/p} L^{-(1+1/p)}; \quad \Theta > \Theta_j\,. \tag{13}$$

Once substituting ℓ with ℓ/N, equation (13) is the same as equation (2) of Urry & Shafer, although it is applicable in a restricted luminosity range. Substituting equation (13) into equation (8) we can derive the observed luminosity function. As in the Urry & Shafer scheme, in the luminosity range $L(\Theta > \Theta_j)$ the beamed LF will approximately be a power law with slope $1 + 1/p$.

For viewing angles $\Theta < \Theta_j$, the enhancement of the luminosity is almost constant, and approaches the value $\bar{R}(0)$. Therefore objects with luminosity $L \sim \ell\bar{R}(0)$ can be seen for lines of sight inside the jet angle. This corresponds to a probability of seeing objects of luminosity $L \sim \ell\bar{R}(0)$ greater than in the Urry & Shafer case. Therefore, in our model, $P(L, \ell)$ is not a power law in the entire luminosity range, but shows an excess in the high-luminosity end.

For $\Theta < \Theta_j$ we can directly derive the approximate luminosity function by setting $\bar{R}(\Theta) = \bar{R}(0) = \text{const}$ in equation (10), and integrating in the range $[0, \Theta_j]$

$$\Phi(L) \sim \Phi_u(\ell)\frac{(1 - \cos\Theta_j)}{\bar{R}(0)}; \quad \Theta < \Theta_j\,. \tag{14}$$

Since the limit in the viewing angles corresponds to a limit in observed luminosities, equation (14) is valid for $L > L_3 = \ell_{\min}\bar{R}(0)$. As in the Urry & Shafer case, the LF of the beamed objects has the same slope of the parents in the high-luminosity end.

Consider the case of a power-law LF of the parents: $\Phi_u(\ell) = \Phi_0\ell^{-B}$. The LF of the beamed objects will have a power-law slope flatter than B for $L \ll L_3$, it will show an excess for $L \leq L_3$, and it will be a power law of slope B above L_3. These features can be seen in Figure 3, where the LF of the beamed population (solid line) as predicted by the wide jet model is shown, together with the LF of the parent sources (dot-dashed line). For illustration $\Phi_u = \ell^{-2}$, $\Gamma = 10$, $\Theta_j = 30°$ and $f = 0.1$ were assumed.

It is interesting to evaluate the ratio, call it R_Φ, of beamed to parent LF at (and above) L_3, in the case of a power law. From equation (14) we derive

$$R_\Phi \equiv \frac{\Phi(L_3)}{\Phi_u(L_3)} = (1 - \cos\Theta_j)\bar{R}(0)^{B-1}\,. \tag{15}$$

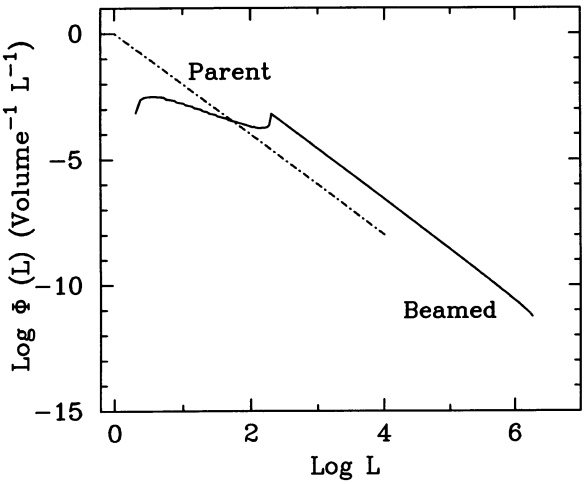

FIG. 3.—Luminosity function of the beamed sources (i.e., $\bar{R} \geq 2$), derived from the parent LF represented by the dot-dashed line, according to the wide jet model. The parent LF has the form $\Phi_u = \ell^{-2}$, and the model parameters are $\Gamma = 10$, $\Theta_j = 30°$, and $f = 0.1$. The predicted features of the beamed LF, i.e., a flat low-luminosity tail, an excess at intermediate luminosity $\sim L_3$ and a power law with the same slope of the parent LF in the high-luminosity part, can be clearly seen.

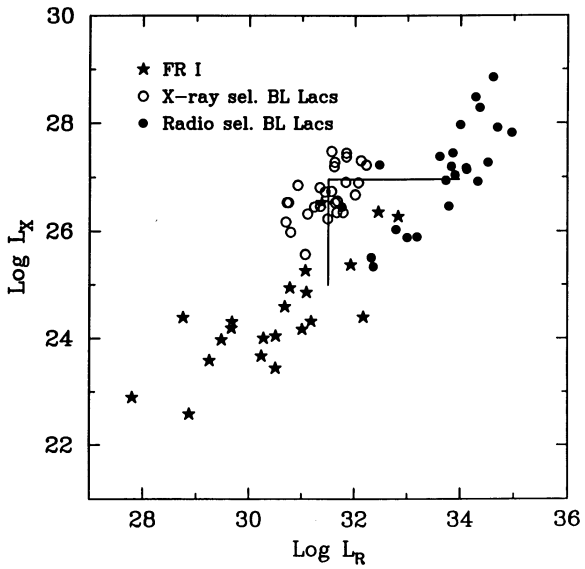

FIG. 4.—X-ray luminosity at 2 keV vs. the (core) radio luminosity at 5 GHz for FR I sources (*stars*), X-ray–selected (*open circles*), and radio–selected (*filled circles*) BL Lac objects from the 3C, Morris et al. (1991), and Stickel et al. (1991) samples, respectively. The L-shaped curve corresponds to changing the line of sight direction according to the "wide" jet model. It is calculated using $\Gamma = 10$, $\Theta_X = 45°$, $p_R = 3$, $p_X = 4$, and $f_X = f_R = 0.1$. Moving along the curve FR I, XBL, and RBL sources are observed.

This ratio can be used to put constraints on the choice of the parameters, once we identify a particular class of sources as the parent population of BL Lac objects (see § 5).

3. BL LAC OBJECTS AS OBJECTS WITH WIDE X-RAY JETS AND NARROW RADIO JETS

Figure 4 shows the observed values of the X-ray luminosity L_X and radio luminosity L_R of the samples of X-ray–selected BL Lac objects (Morris et al. 1991), radio-selected BL Lac objects (Stickel et al. 1991), and FR I radio galaxies of the 3C sample (Fabbiano et al. 1984).

It is clear that the different samples populate different regions of the $L_X - L_R$ plane, corresponding to different ratios L_X/L_R. If the luminosity enhancements in the two bands were proportional to each other there would be no way of connecting the same parent population to both XBLs and RBLs.

Let us suppose that the relativistic jets of BL Lac objects have distinct emission regions. The inner jet, producing the X-rays, has an opening angle $\Theta_j = \Theta_X$ much greater than Θ_c, and Θ_j decreases along the jet, reaching Θ_c in the outer, radio-emitting, parts (see Fig. 1). Then, using the results of the previous section, we can compute L_X and L_R as a function of the viewing angle Θ, obtaining, for a fixed value of the intrinsic luminosities, a track in the $L_X - L_R$ plane which corresponds to the same object viewed at different angles. A track corresponding to $\Gamma = 10$, $\Theta_X = 45°$, $f_X = f_R = 0.1$ is shown in Figure 4. The parameters were chosen so that the shape of the track (straight up first, followed by a right turn) is such that we can now connect "typical" FR I luminosities to X-ray–selected luminosities and radio-selected luminosities, varying only the viewing angle.

The ratio of the enhancement factors due to beaming in the radio and X-ray bands, $\bar{R}_R/\bar{R}_X$, for the same values of the parameters, is shown as a function of the viewing angle in Figure 5. Due to the different dependence of the radio and X-ray luminosities on Θ, the curve has three distinct regions which define three intervals for the viewing angle.

At very large angles, $\Theta > \Theta_X$, the unbeamed luminosities dominate, that is, $\bar{R}(\Theta) \simeq 1$ for both bands. This region corresponds to unbeamed objects, that is to the parent population, possibly FR I radio galaxies.

When Θ approaches Θ_X, the observed X-ray luminosity is enhanced by beaming and increases rapidly to its flat top value (see Fig. 2), while the observed radio luminosity stays almost constant being still dominated by the isotropic component. Thus, for $\Theta \leq \Theta_X$, $\bar{R}_R/\bar{R}_X$ goes through a flat minimum.

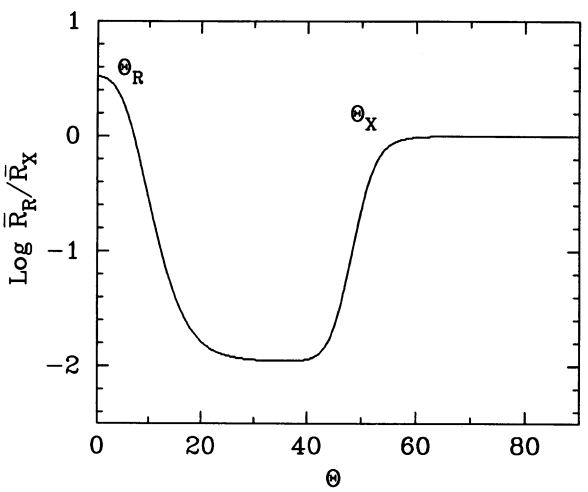

FIG. 5.—Relative ratio of the radio to X-ray amplification factors $\bar{R}_R/\bar{R}_X$ as a function of the viewing angle Θ according to the wide jet model. The adopted parameters are $\Gamma = 10$, $\Theta_X = 45°$, $f_X = f_R = 0.1$. At large angles we are observing out of the X-ray cone, and therefore we can see the unbeamed luminosity. For smaller $\Theta \leq \Theta_X$ we start to see a beamed X-ray luminosity and decreasing further the angle ($\Theta \sim \Theta_R$), also the radio luminosity is beamed, while the X-ray one remains almost constant.

Objects in this range of viewing angles would be classified as beamed if observed in X-rays. We identify these sources as the XBLs. Clearly the critical angle separating the parent and the beamed population depends on the precise shape of the curve, which depends on f_X, and its choice is to some extent arbitrary. For simplicity we will use Θ_X as the dividing angle. An alternative choice (adopted by Padovani & Urry 1990) is to use the angle for which $\bar{R}_X = 2$, that is, the beamed X-ray luminosity is equal to the isotropic one.

For still smaller angles, $\bar{R}_X$ remains almost constant (the line of sight is within the large X-ray jet), but, when Θ approaches Θ_c, the radio luminosity starts to be enhanced by beaming. Then $\bar{R}_R$ rapidly increases until $\Theta \sim 0°$ and $\bar{R}_R/\bar{R}_X$ reaches a maximum.

The shape of the rise of $\bar{R}_R$ again depends on f_R but is in general less abrupt than that of $\bar{R}_X$. The problem of exactly defining Θ_R is the same as discussed above for Θ_X. Because of the more gradual rise of $\bar{R}_R$ we will assume $\Theta_R = 2\Theta_c$ (independent of f_R). For $\Theta < \Theta_R$ both the X-ray and the radio luminosities are enhanced, and these objects would be classified as beamed in both bands. All the RBLs should satisfy the above criterion. This implies that, from the point of view of the energy distribution, X-ray surveys would be unbiased toward detection of RBLs.

The X-ray and radio LFs for XBL- and RBL-type sources can be computed using the results of § 2. For RBLs we have $0 < \Theta < \Theta_R$ and for XBLs $\Theta_R < \Theta < \Theta_X$. In order to allow a qualitative insight in the features of the model, we assumed a simple form of the LF of the (unbeamed) parent population $\Phi_u \propto \ell^{-2}$, with arbitrary normalization, $\Gamma = 10$, $\Theta_X = 30°$, $f_R = f_X = 0.1$. The resulting LFs in the X-ray and radio bands are shown in Figures 6*a* and 6*b*. The dot-dashed, continuous, and dashed lines represent the LF of the parent population and the XBL and RBL sources, respectively.

In the X-ray band (Fig. 6*a*) the LFs of XBLs and RBLs extend to the same maximum luminosity, of the order of $\ell_{\max} \bar{R}(0)$. By definition the XBL class includes objects observed at $\Theta \leq \Theta_X$, and therefore the LF of XBLs, extends only above L_3. As described in § 2.2, the number density of XBLs exceeds the corresponding density predicted in the parallel velocity scheme. In the X-ray band RBLs are similar to XBL sources: their LF differs from that of XBLs just for the lower normalization, due to the smaller angle subtended by RBLs compared to XBLs. The ratio of the number densities of XBLs and RBLs is therefore given by

$$R_N \equiv \frac{1 - \cos(\Theta_X)}{1 - \cos(\Theta_R)} - 1 \qquad (16)$$

and represents an essential constraint on the model. In order to estimate this ratio the X-ray LF of RBL objects will be derived in the next section.

From Figure 6*b* it appears that the radio LF of XBLs is shifted toward lower radio luminosities with respect to that of RBLs. In fact their radio amplification is lower. Note that the amplification is estimated from equation (1) also in the radio band (for $\Theta_R = 2\Theta_c$), and it is consequently smaller than the enhancement obtained in the case of the parallel velocity flow.

Because of the wider solid angle, the XBLs are more numerous than the RBLs, for a given unbeamed luminosity. This can be seen at the low end of the LF. However, the lower amplification dominates over the density effects in the high radio luminosity regime, thus, above the break of the LF associated with the minimum luminosity of the parents, XBLs are *less* than RBLs, while they exceed the number of RBLs at very low radio luminosities.

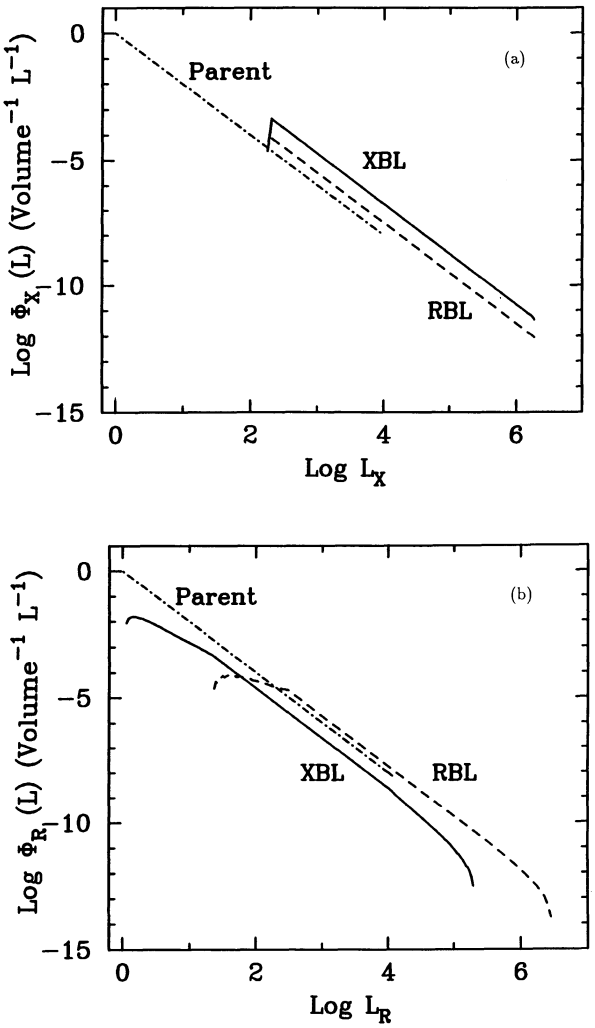

FIG. 6.—Luminosity functions in the X-ray (*a*) and radio (*b*) band for XBL (*solid line*) and RBL (*dashed line*) as predicted by the model. The LFs of the parent population (*dot-dashed line*) have been assumed to be of the form $\Phi_u = \ell^{-2}$, and the model parameters are $\Gamma = 10$, $\Theta_X = 30°$, $f_X = f_R = 0.1$.

In summary: the model predicts that for a fixed X-ray luminosity, XBL sources are more numerous than RBLs, while the opposite is predicted for a fixed radio luminosity, above the break in the radio LF.

4. LUMINOSITY FUNCTIONS OF FR I RADIO GALAXIES AND BL LAC OBJECTS FROM OBSERVATIONS

We now examine the radio and X-ray observations of FR I radio galaxies, XBLs, and RBLs in view of applying the model outlined above. From the literature we derive the LFs of FR I radio galaxies in both bands, the X-ray LF of X-ray–selected BL Lac objects, and the radio LF of radio-selected BL Lac objects. We determine below for the first time the X-ray LF of radio-selected BL Lac objects and the radio LF of X-ray–selected BL Lac objects.

The values $H_0 = 50$ km s^{-1} Mpc^{-1} and $q_0 = 0$ have been used.

FR I—The differential LF of FR I radio galaxies in the X-ray (0.3–3.5 keV) and radio (5 GHz) bands have been computed by Padovani & Urry (1990) and Urry et al. (1991c).

In the X-ray band we adopt their analytical fit $\Phi_X(\ell_X) = 2.4 \times 10^{49} \ell_X^{-2.1}$ [Gpc^{-3} ℓ_X^{-1}] between $\ell_{min} = 2.6 \times 10^{40}$ and $\ell_{max} = 1.6 \times 10^{44}$ [ergs s^{-1}]. In the radio band we consider the LF as derived from the 2 Jy sample (Wall & Peacock 1985), $\Phi_R(\ell_R) = 9.2 \times 10^{43} \ell_R^{-2.33}$ [Gpc$^{-3}\ell_R^{-1}$], between $\ell_{min} = 7.9 \times 10^{29}$ and $\ell_{max} = 6.3 \times 10^{33}$ [ergs s^{-1} Hz^{-1}]. At luminosities lower than ℓ_{min} the luminosity function is very uncertain (see Urry et al. 1991c for further discussion on this point), moreover the X-ray data for sources below ℓ_{min} are scarce. We will therefore limit our analysis to the luminosity ranges mentioned above and discuss the relevant consequences.

X-ray–selected BL Lac objects—The sample of the X-ray–selected sources is extracted from the *Einstein* Medium Sensitivity Survey (Gioia et al. 1990; Stocke et al. 1991). It contains objects selected on the basis of the equivalent width (<5 Å) of any emission line and a maximum contrast (<25%) in the Ca II break. We have considered the complete subsample having X-ray flux $\geq 5 \times 10^{13}$ ergs s^{-1} cm^{-2} (in the 0.3–3.5 keV band) and declination $\geq -20°$, as defined in Morris et al. (1991). The subsample contains 22 objects, all of which have been observed at 5 GHz with the VLA and have a firm redshift. For the X-ray–selected objects we assume a spectral index $\alpha_X = 1$ (Maccacaro et al. 1988; Worrall & Wilkes 1990) and $\alpha_R = 0$ (Morris et al. 1991). The X-ray LF of this sample is derived in Morris et al. (1991).

Radio-selected BL Lac objects—The radio-selected BL Lac sample is that of Stickel et al. (1991). It contains 34 objects with flux ≥ 1 Jy at 5 GHz, selected from the sample of Kühr et al. (1991) on the basis of the flat spectral index ($\alpha_R \leq 0.5$), optical magnitude $m_v \leq 20$, and rest frame equivalent width (<5 Å). For the radio-selected sample the redshift information is not complete. Only 25 objects have a measured redshift, two of which are uncertain. Four of the remaining sources have a lower limit on the redshift, based on the presence of absorption lines, and five have a rough lower limit ($z > 0.2$) derived from their stellar appearance (Stickel et al. 1991). For the construction of the X-ray LF of the radio-selected sources we have considered these lower limits as actual estimates. Using larger values (e.g., the mean value of the sample, $\langle z \rangle = 0.56$) the corresponding LF slightly increases at high luminosities (Caccianiga 1993). The radio LF of this sample is derived in Stickel et al. (1991).

The X-ray fluxes of the radio selected BL Lac objects are taken from the compilation of Padovani (1992) and are available for 28 objects. The X-ray LF of the radio-selected objects is derived from these 28 sources.[6] We assume a radio spectral index equal to the mean value of the sample, $\alpha_R = -0.27$ (Stickel et al. 1991), and a X-ray spectral index $\alpha_X = 1$ (Padovani 1992).

For the derivation of the X-ray LF of the radio-selected objects and the radio LF of the X-ray–selected ones we follow the same procedure, described in detail by Avni & Bahcall (1980), concerning the coherent analysis of a set of independent samples. In both cases the maximum distance at which a given object could have been detected, used for computing V_a, is derived from the luminosity and flux limits in the band of selection, while the luminosity bins for which the space density is computed refer to the complementary band.

[6] We have normalized the X-ray LF simply by reducing the sky coverage of a factor 28/34.

The test V_e/V_a shows a negative X-ray evolution for the X-ray–selected BL Lac objects (Morris et al. 1991) and a slightly positive radio evolution for the radio-selected, although consistent with zero evolution (Stickel et al. 1991). According to the unified picture we consider the same evolution for the radio- and X-ray–selected BL Lac objects in the same band. Moreover, for the sake of simplicity we assume the closest evolution parameters in the two bands permitted by the confidence intervals of the evolutionary parameters. Thus for both samples we assume no evolution in the radio band, while in the X-ray band we consider a pure luminosity evolution of the form $L_X(z) = L_X(0)(1 + z)^\gamma$, with $\gamma = -1.5$, which is the minimum value in the 2 σ confidence range found by Morris et al. (1991). This choice implies that the ratio L_X/L_R increases with cosmic time in the same way for the two groups, the increase being the minimum compatible with the available data.

The model is intended to account for the relative properties of X-ray– and radio-selected BL Lac objects at a fixed redshift, and we will fix the model parameters by considering the LF at zero redshift (local LF), calculated using values of L and V_a corrected by the minimum evolution described above. The suggested evolution of the L_X/L_R ratio, if confirmed by larger samples allowing a direct determination of the LFs at different redshifts, may be interpreted as a variation with cosmic epoch of the physical parameters involved in the model.

The X-ray LFs and the radio LFs are presented in Figures 7*a* and 7*c*, respectively. The open circles refer to the X-ray–selected sources, while filled circles indicate the radio-selected sources. For comparison we also report in Figures 7*b* and 7*d*, the LFs derived with the evolution parameters of the best fits found by Morris et al. (1991) and Stickel et al. (1991) in the X-ray and radio bands, respectively. In the latter case we assumed an X-ray luminosity evolution of the form $L_X(z) = L_X(0)(1 + z)^\gamma$, with $\gamma = -7.0$ and a radio luminosity evolution of the form $L_R(z) = L_R \exp(T(z)/\tau)$, with $\tau = 0.32$ ($T(z)$ is the lookback time), both for X-ray– and radio-selected BL Lac objects. The strong negative evolution in the X-rays affects the corresponding luminosity function, as can be seen by comparing Figures 7*a* and 7*b*. For a fixed X-ray luminosity, the average ratios of the number densities of X-ray– and radio-selected objects are ~ 8 and ~ 25 for the case of no evolution and best-fit evolution, respectively.

The error bars are determined by

$$\sigma_\pm = (\epsilon_\pm - N)\left(\frac{1}{N}\sum_i V_{a,i}^{-2}\right)^{1/2}, \qquad (17)$$

where $\epsilon_\pm$ are the Poissonian upper and lower limits (tabulated, e.g., in Gehrels 1986), N is the total number of objects in a given bin of luminosity, and $V_{a,i}$ is the "available" volume for each source. The expression weighs each observation by its contribution to the sum and takes into account the case of small statistics ($N \leq 20$). It is useful when the number of objects in each bin is very small and when the values of $1/V_a$ change significantly within a single bin. For a large value of N, equation (17) turns into that generally used (Marshall 1985).

5. RESULTS

Assuming FR I as the parent population of both XBLs and RBLs, we can now use the derived LFs to quantitatively constrain the model parameters.

Given the LFs of the parent population in the radio and X-ray bands, these are the beaming factor Γ, the opening angle

of the jet in the X-ray–emitting region, Θ_X, and the fraction of beamed to unbeamed power in the X-ray and radio bands, that is, f_X and f_R. The radio-emitting plasma is assumed to be fully collimated with $\Theta_R = 2\Theta_c \sim 2/\Gamma$.

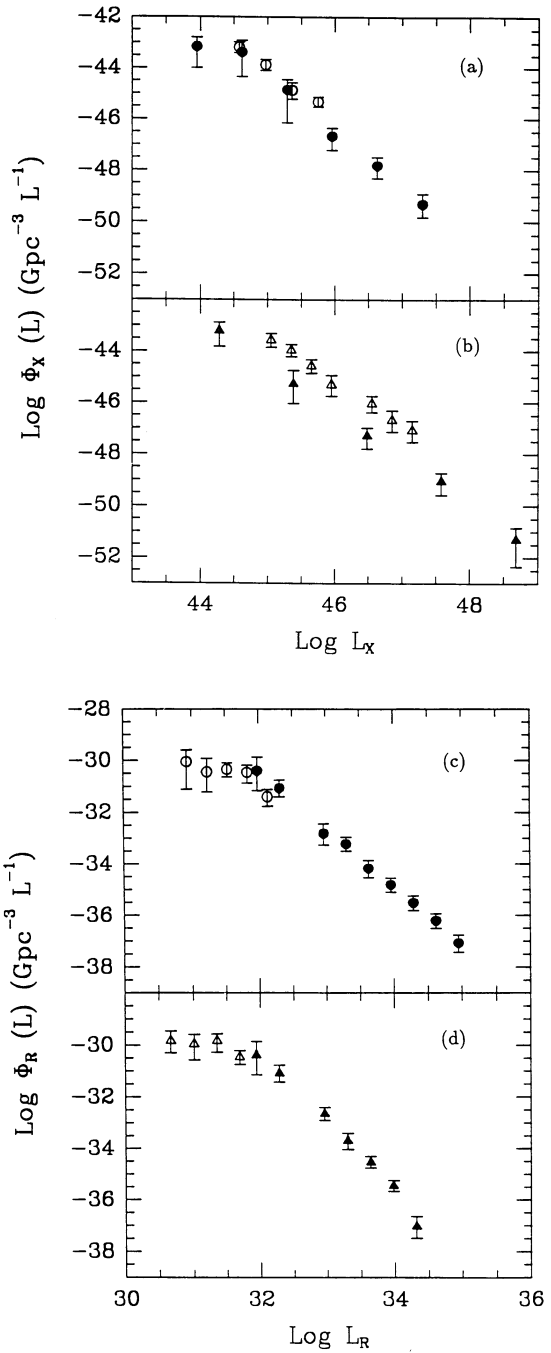

FIG. 7.—Differential luminosity functions of X-ray–selected and radio-selected BL Lac objects derived from the samples of Morris et al. (1991) and Stickel et al. (1991) for different values of evolution. (*a*)–(*b*) The X-ray LFs computed assuming: (*a*) a minimum evolution consistent with the data in the X-ray band and no evolution in the radio band (see text); the XBLs and RBLs are represented as open and filled circles, respectively; (*b*) the best-fit evolution found by Morris et al. (1991) and Stickel et al. (1991); the XBLs and RBLs are represented as open and filled triangles, respectively. (*c*)–(*d*) The radio LFs for the case of (*c*) no evolution and (*d*) best-fit evolution. Symbols are the same as (*a*) and (*b*).

The observational constraints which the model must satisfy are discussed below.

5.1. *Amplification Ratios*

The maximum amplification ratios $R_{\max R,X} \equiv L_{\max R,X}/\ell_{\max R,X}$ can be written, for $\Gamma \gg 1$, as (see eqs. [3], [6])

$$R_{\max R} \sim 1 + 2f_R\Gamma^3 ,$$

$$R_{\max X} \sim 1 + \frac{8f_X\Gamma^2}{(1 - \cos\Theta_X)} \qquad (18)$$

in the radio and X-ray bands, respectively. They represent two constraints on the model parameters. Coherently with the proposed scheme they can be estimated from Figure 4: comparing X-ray–selected BL Lac objects with FR I galaxies *with the same radio power* we deduce $R_{\max X} \simeq 100$, while comparing X-ray–selected BL Lac objects with radio-selected BL Lac objects with the same X-ray power we deduce $R_{\max R} \simeq 300$. These numbers are obtained by assuming a proportionality relation between L_X and L_R for each group and taking the ratios of the best-fitted regression lines.

The main uncertainties here concern the selection effects which may bias the different samples and are difficult to assess. However, an important, independent estimate for $R_{\max R}$ is discussed by Kollgaard et al. (1992), using new measurements of the extended ratio emission of BL Lac objects. These allow a comparison of BL Lac objects and FR I *with the same extended power* from which $100 \leq R_{\max R} \leq 1000$ is derived. The agreement of the two estimates of R_R is per se a consistency argument for our scheme.

We note that the radio-selected BL Lac sample extends to higher X-ray luminosities than the X-ray–selected sample (see Fig. 4) contrary to the model predictions. Several effects may contribute to this apparent discrepancy: the maximum luminosity of the X-ray–selected BL Lac objects may be limited by the solid angle of the EMSS survey, in addition some of the more luminous BL Lac objects may derive from FR II sources, as shown by Kollgaard et al. (1992). Such sources, when observed at intermediate angles ($\Theta_X > \Theta > \Theta_R$), may show some line emission and therefore would not be classified as BL Lac objects. Furthermore, we are comparing objects at different redshifts, and the evolutionary corrections are uncertain. Thus we provisionally assume that the different maximum luminosity is a spurious effect.

5.2. *Relative Number of XBLs and RBLs*

The relative number of XBLs and RBLs observed in X-ray and radio surveys is a crucial constraint for the model.

As shown in Figure 6*a* our scheme predicts the same shape and extent of the X-ray luminosity function for XBLs and RBLs, with only a different normalization. In fact it is worth recalling that the angle Θ_R separates objects with high and low amplification in the radio luminosity, *irrespective* of the X-ray luminosity. A fraction of the X-ray–selected objects proportional to the associated solid angle should have $\Theta < \Theta_R$ and therefore a high radio luminosity. Thus for a given X-ray luminosity the ratio of XBLs and RBLs is given by equation (16).

In an unbiased and complete *X-ray sample*, the ratio of radio-weak (XBLs) to radio-loud objects (RBLs) should determine R_N. No radio-loud object is detected in the EMSS X-ray–selected sample. On the other hand, EMSS fields avoid known sources, which may introduce a bias against radio-loud

objects. We therefore derive this ratio from the comparison of the X-ray LFs for XBLs and RBLs derived in § 4 by fitting them with power laws with the same index. The ratio is estimated to be ~ 8 in the assumption of minimal evolution.

Note that the actual data points for the X-ray–selected sample do not reach the same maximum luminosity as for the radio-selected sample. As discussed above this is a potential difficulty; on the other hand, richer samples are needed to assess this point. It should be remembered that, since an X-ray survey is expected to detect both XBLs and RBLs the observed LF of the X-ray sample should be compared with the sum of the XBL and RBL luminosity functions. However, provided that the ratio is large, this correction is minor.

A comparison of XBLs and RBLs in the radio band is not straightforward because of the different radio properties. The radio LF of X-ray–selected objects is much flatter (best-fit slope 1.1 ± 0.4) than that of radio-selected objects (best-fit slope 2.2 ± 0.1). A single power-law fit to the combined radio LFs, though not unacceptable, gives a slope of 1.9 ± 0.1, flatter than that of the assumed parent population. If the slopes of the parent and beamed populations are required to agree, then the radio LF of X-ray–selected objects clearly indicates a flattening. Since, however, the procedure of derivation of the radio LF of XBLs could generate spurious changes of slopes, due to the finite sampling of luminosities in the selection band, coupled with the observed dispersion in the L_R/L_X ratio, larger statistics will be essential in determining the reality of this flattening.

If the effect is real, the "break" at $\sim 10^{32}$ ergs s^{-1} Hz^{-1} in the total (XBL + RBL) LF may be interpreted as due to a threshold luminosity in the LF of the parent population. This does not imply that the LF of FR I radio galaxies should not extend to lower luminosities, but only that lower luminosity FR I sources may not harbor active relativistic jets. We recall that the radio luminosities considered here refer to the nucleus of the radio source.

5.3. *Relative Number of FR I and BL Lac Objects*

As shown in § 2, the ratio R_Φ of beamed to parent luminosity functions, evaluated above the luminosity L_3, is given by equation (15). There are two constraints of this type, one from the X-ray LFs of FR I and X-ray–selected BL Lac objects, one from the radio LFs of FR I and radio-selected BL Lac objects. From the observed LFs discussed in the previous section we derive $R_{\Phi,X} \simeq 20$ and $R_{\Phi,R} \simeq 2$.

5.4. *Derived Parameters*

We have discussed five constraints, $R_{\max X}$, $R_{\max R}$, R_N, $R_{\Phi,X}$, $R_{\Phi,R}$ for our four parameters: Γ, Θ_X, f_X, f_R. The model is overconstrained; however, there are uncertainties in the values estimated from the observations which are difficult to quantify. In particular the values of $R_{\max X}$ and $R_{\max R}$ are relatively large numbers, and they are raised to exponents $(B_{X,R} - 1)$ where $B_{X,R}$ is the slope of the relevant luminosity function. Thus the uncertainty in $B_{X,R}$ enters in a significant way. Without entering into a sophisticated analysis of uncertainty propagation, we proceed as follows: assume a value for $R_{\max R}$. Neglecting errors on $B_{X,R}$ and on the observed ratios, this fixes a value of $R_{\max X}$. We then solve the remaining equations exactly for Γ, Θ_X, f_X, f_R. For a given $\ell_{\min}$ of the parent population a "break" is predicted in the radio LF. Requiring the break to fit the observed flattening we derive $\ell_{\min}$ accordingly. Unfortunately there is no strong observational constraint on $\ell_{\min}$. However, the fact that we can derive a consistent set of parameters adopting $\ell_{\min}$ from the LF of FR I (see § 4) suggests that indeed the nature of FR I sources may be different below and above this threshold.

The constraints discussed above determine the following set of parameters: $\Gamma = 29$, $\Theta_X = 13°$, $f_R = 6 \times 10^{-3}$, and $f_X = 5 \times 10^{-3}$, corresponding to $R_R = 160$, $R_X = 430$. For consistency we verified that all the sources observed inside Θ_R and Θ_X are "beamed" objects (i.e., $\bar{R} > 2$). Higher values of $R_{R,X}$ would lead to higher values of Γ and smaller angles, while lower values of $R_{R,X}$ (at most by a factor 2) would have the opposite effect.

The differential LF in the X-ray and radio bands computed from the model, with the parameters derived above, are shown in Figure 8. Continuous lines refer to XBLs, dashed lines to RBLs. We also report the observed LF: FR I radio galaxies are represented by the dot-dashed lines, while X-ray–selected BL Lac objects are indicated by open circles and radio selected by filled circles.

The values above have been derived assuming the minimum amount of negative evolution in X-rays consistent with the data (see § 4); they do not change dramatically in the case of stronger negative evolution.

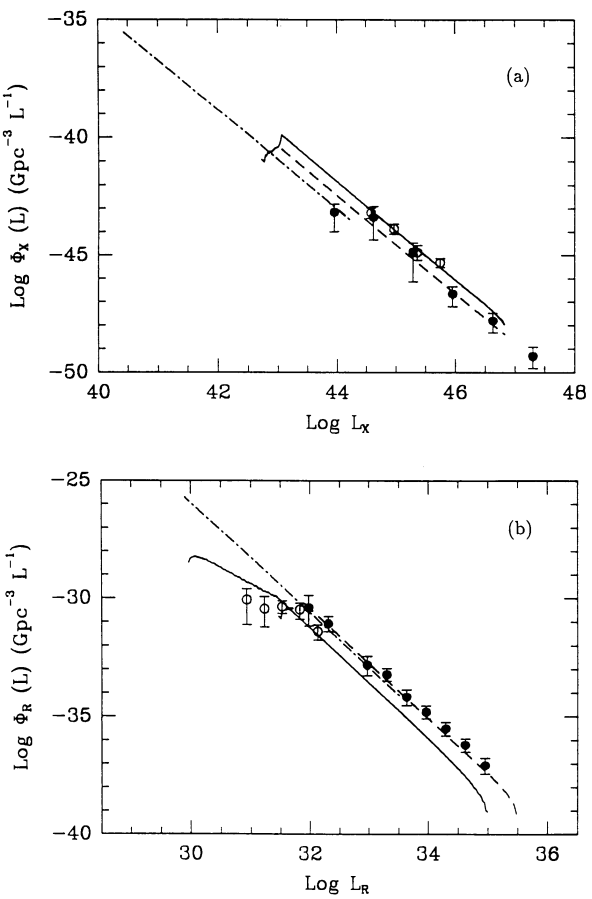

FIG. 8.—Differential X-ray luminosity function of BL Lac objects calculated assuming FR I radio galaxies as parent population (the LF of which is shown as dot-dashed line), for $\Gamma = 29$, $\Theta_X = 13°$, $f_X \simeq f_R \simeq 5 \times 10^{-3}$. The continuous and dashed lines represent the XBL and RBL luminosity functions derived from the model, respectively. The LFs (no evolution) of XBLs (*open circles*) and RBLs (*filled circles*) are also reported (as in Fig. 7*a*). (*b*) As in (*a*), in the radio band. The circles represent the LF shown in Fig. 7*c*.

The derived value of Γ substantially exceeds the estimate of the bulk Lorentz factor for a large sample of sources, including BL Lac objects, by Ghisellini et al. (1993), based on the SSC theory and the observed superluminal velocities.

The main constraint that determines a large value of Γ in the present model is the small ratio of BL Lac objects to FR I sources at a given radio luminosity. For a given amplification ratio R_R it determines the width of the radio cone, which turns out to be very small. We have considered the possibility that only a fraction of the FR I radio galaxies are active and give rise to the BL Lac phenomenon. We have then assumed the typical value of the bulk Lorentz factor $\Gamma = 10$ estimated by Ghisellini et al. (1993), and in this case we obtain a good fit using $f_R = 0.2$, $f_X = 0.5$, and $\Theta_X = 41°$ if only 1/10 of FR I radio galaxies are presently active. In this case the X-ray jet opening angle is in agreement with the average viewing angle estimated by Ghisellini et al. (1993) for BL Lac objects.

Interestingly, an independent but similar line of argument has lead Kollgaard et al. (1992) to suggest the possibility that the progenitors of BL Lac objects are FR I sources with relatively radio-bright nuclei. In fact the activity of the nucleus may be short lived and recurrent, while the extended power may represent the "integrated" result of the former.

At this stage, however, this hypothesis adds to some relevant uncertainties and complications of the simple procedure we followed, for example:

1. The hypothesis that f is constant for all sources may not hold, and some of the beamed object, instead of having a large Γ, may be characterized by a large f. Furthermore, the simple picture presented here can be extended to include the possibility of a distribution, rather than a single value, of the bulk Lorentz factor (as assumed by Urry & Padovani 1991).

2. The LF of FR I, XBL, and RBL sources are based on small samples. All the ratios are affected by the evolutionary hypotheses. In this respect the 90 BL Lac objects expected from the slew survey (at least nine of which are radio selected) will allow substantial progress as well as the likely advance in the study of X-ray properties of FR I sources from *ROSAT* observations.

6. SUMMARY AND CONCLUSIONS

We have considered the possibility that the bimodal spectral and spatial distributions of X-ray– and radio-selected BL Lac objects are both accounted for if X-rays are beamed in a wider cone than the radio emission. This may occur if the bulk Lorentz factor Γ of the X-ray–emitting plasma is smaller than that of the radio-emitting plasma or if in the former region the flow has high Γ but is less collimated. The latter case is treated here in detail. The resulting, aspect-dependent flux enhancement shows a flat top, lower but wider in angle than that corresponding to a narrow jet with the same Γ.

For a line of sight inside the narrower opening angle of the radio jet Θ_R, the radio and X-ray fluxes are both enhanced, giving rise to a RBL source, while at angles larger than Θ_R but smaller than the X-ray opening angle Θ_X, only the X-ray flux is amplified, and the source would appear as an XBL object. Consequently, in an X-ray–selected sample, XBL sources are expected to be more numerous than RBLs, due to the fact that the X-ray enhancement is the same (flat top), but the subtended solid angle is wider.

From the available data we have computed the LF in the X-ray and radio bands, for the radio- and X-ray–selected BL Lac samples, respectively. These add to the previously known LFs, in the radio for the radio-selected and in the X-ray for the X-ray–selected samples.

We have then compared the LFs predicted by the model in either band for the two samples with those observationally determined, assuming FR I radio galaxies as parent population. From this comparison, mainly based on the relative number densities of these three classes of sources, we have determined the model parameters.

Although the parameter determination depends on assumptions and uncertainties about the LFs, it seems inevitable that this procedure leads to very high values of the bulk Lorentz factor Γ, the main constraint being the small number of radio-selected BL Lac objects with respect to the parent radio galaxies.

In a recent study of relativistic bulk motion in AGNs, based on direct physical arguments, Ghisellini et al. (1993) determined an average value of $\Gamma \simeq 10$ for BL Lac objects. The only possibility of reconciling this value of Γ with the scheme presented here is to hypothesize that only about 10% of FR I radio galaxies currently contain active relativistic jets. In this hypothesis, for a bulk Lorentz factor $\Gamma \sim 10$, the derived jet opening angles are $\Theta_X \sim 40°$ (corresponding to ~ 3 ster for a double jet) and $\Theta_R \sim 11°$, according to a numerical ratio of XBL and RBL objects (in X-ray–selected samples) of ~ 10. The fraction of unbeamed radiation which is amplified by beaming is of the order of few tenths in both bands.

In summary, the basis facts for which our description can account are the following:

The existence of two populations of BL Lac objects within the unification model for BL Lac objects and FR I radio galaxies. Our scheme explains why XBLs are more abundant than RBLs in X-ray surveys, while the opposite is obtained from radio searches, and *at the same time* why the spectral distributions of the sources belonging to these two classes are different, leading to a dichotomy in the value of α_{RX} for the two populations. This "bimodal" effect (see Fig. 4) is related to the flat-top shape of the flux-enhancement versus angle relation which is a characteristic feature of the wide jet model.

The sequence of "beamed sources: FR I–XBL–RBL, corresponds to a decreasing viewing angle in a way similar to the sequence: FR II-lobe dominated-core dominated quasars as suggested by Ghisellini et al. (1993).

Urry & Padovani considered separately the relation between FR I galaxies and X-ray–selected BL Lac objects on one hand and radio-selected BL Lac objects on the other, inferring a different value of the bulk Lorentz factor Γ for the two bands. Thus the basic point that the degree of beaming increases with decreasing frequency seems rather firmly established.

The "wide jet" model here proposed does not need an acceleration mechanism smoothly operating over large distances, as requested for the accelerating jet model. However, the physics of (re)collimation of the jet is poorly known. An increasing collimation can be obtained because the jet is pressure-confined by the external gas, assuming a parabolic shape, or because the plasma moving at larger angles suffers more Compton drag, and only the inner part of the jet can survive during the propagation. The geometry of an intense and ordered magnetic field component could also determine the collimation (e.g., Begelman 1992). Thus it is difficult at present to favor either model on the basis of physical arguments.

While "statistically" the two models may be very close, a significantly different prediction concerns the emission properties. In fact, in the wide jet model, the observed X-ray flux derives from highly relativistic plasma. Therefore we would expect that even small variations in the comoving luminosity can result in strong and rapid variations of the observed luminosity, while these effects should be less violent in the accelerating jet model.

An indication of large Γ in the X-ray–emitting region is the recent detection of several BL Lac objects at energies above 100 MeV by the instrument EGRET aboard the *Compton Gamma Ray Observatory*. In fact, beaming of the high-energy radiation makes the source transparent to the γ-rays which can escape the source without suffering photon-photon collisions with target X-rays. Furthermore, this helps to explain the apparent extraordinary luminosity output in the γ-ray band (see, e.g., Maraschi, Ghisellini, & Celotti 1992).

Finally, as already stressed, the model parameters derived from the comparison with present observations should be considered with caution. A larger and unbiased complete sample of BL Lac objects observed in the X-rays and in the radio band, allowing a direct determination of the absolute properties and relative density of XBLs and RBLs in the same sample, would be of great value. The *Einstein* Slew Survey may soon provide such sample.

A.C. acknowledges the Italian MURST and the Royal Society for financial support. This work has received partial financial support from the Italian Space Agency.

APPENDIX A

In this appendix we find analytically the factor $R(\Theta)$ of equation (1), for integer values of p.

We first solve the integral, let us call it $I(\theta, \Theta)$, in the variable ϕ. We have

$$I(\theta, \Theta) \equiv \int_0^{2\pi} \frac{d\phi}{[1 - \beta\,(\sin\Theta \sin\theta \cos\phi + \cos\Theta \cos\theta)]^p} = \frac{2}{b^p} \int_0^{\pi} \frac{d\phi}{(a - \cos\phi)^p}\,, \tag{A1}$$

where

$$b \equiv \beta \sin\Theta \sin\theta \qquad c \equiv 1 - \beta \cos\Theta \cos\theta \qquad a \equiv c/b\,. \tag{A2}$$

The calculation of the integral $I(\theta, \Theta)$ can be reduced to the calculation of I_1:

$$I(\theta, \Theta) = \frac{2}{b^p} \frac{1}{(1-p)(2-p)\ldots(-1)} \frac{d^{p-1} I_1}{da^{p-1}}\,,$$

where

$$I_1 = \int_0^{\pi} \frac{d\phi}{(a - \cos\phi)}\,. \tag{A3}$$

With the two changes of variable

$$\cos\phi = \frac{1 - t^2}{1 + t^2} \qquad x = t\left(\frac{a+1}{a-1}\right)^{1/2} \tag{A4}$$

we obtain

$$I_1 = \frac{4}{\sqrt{a^2 - 1}} \left[\operatorname{arctg}\left(\sqrt{\frac{a+1}{a-1}} \sqrt{\frac{1 - \cos\phi}{1 + \cos\phi}}\right)\right]_0^{\pi} = \frac{2\pi}{\sqrt{a^2 - 1}}\,. \tag{A5}$$

Substituting in equation (A3) we obtain, for $p = 3$

$$I(\theta, \Theta) = \frac{1}{2} \frac{1}{b^3} \frac{d^2}{da^2} I_1 = \frac{\pi}{b^3} \frac{2a^2 + 1}{(a^2 - 1)^{5/2}} = \pi \frac{(b^2 + 2c^2)}{(c^2 - b^2)^{5/2}}\,, \qquad p = 3\,, \tag{A6}$$

while, for $p = 4$, we have

$$I(\theta, \Theta) = -\frac{1}{6} \frac{1}{b^4} \frac{d^3}{da^3} I_1 = \frac{\pi}{b^4} \frac{a(2a^2 + 3)}{(a^2 - 1)^{7/2}} = \pi c \frac{(3b^2 + 2c^2)}{(c^2 - b^2)^{7/2}}\,, \qquad p = 4\,. \tag{A7}$$

The last two equalities in eqs. (A6) and (A7) avoid the vanishing of the denominator at $\Theta = 0$.

We do not report the analytic integration of $I(\theta, \Theta)$ in the variable θ. It reduces to the integration of rational functions $F_3(\cos\theta) = Q_1(\cos\theta)/Q_2^{5/2}(\cos\theta)$ (for $p = 3$) and $F_4(\cos\theta) = Q_3(\cos\theta)/Q_4^{7/2}(\cos\theta)$ (for $p = 4$), where $Q_i(\cos\theta)$ are second-order polynomials, which can be solved substituting $t = \cos\theta - \cos\Theta/\beta$.

REFERENCES

Abraham, R. G., McHardy, I. M., & Crawford, C. S. 1991, MNRAS, 252, 482
Antonucci, R. R. J., & Ulvestad, J. S. 1985, ApJ, 294, 158
Avni, Y., & Bahcall, J. N. 1980, ApJ, 235, 694
Begelman, M. C. 1992, in Jets in Extragalactic Radio Sources, ed. H.-J. Röser et al. (Berlin: Springer), in press
Blandford, R. D. 1987, in Superluminal Radio Sources, ed. A. Zensus & T. Pearson (Cambridge: Cambridge Univ. Press), 310
Blandford, R. D., & Rees, M. J. 1978, in Pittsburgh Conference on BL Lac Objects, ed. A. N. Wolfe (Pittsburgh: Pittsburgh Univ. Press), 328
Browne, I. W. A. 1983, MNRAS, 204, 23P
Caccianiga, A. 1993, Laurea thesis, Univ. Milano
Fabbiano, G., Miller, L., Trinchieri, G., Longair, M., & Elvis, M. 1984, ApJ, 277, 115
Garrington, S. T., Leahy, J. P., Conway, R. G., & Laing, R. A. 1988, Nature, 331, 147
Gehrels, N. 1986, ApJ, 303, 336
Ghisellini, G., & Maraschi, L. 1989, ApJ, 340, 181
Ghisellini, G., Padovani, P., Celotti, A., & Maraschi, L. 1993, ApJ, 407, 65
Gioia, I. M., Maccacaro, T., Schild, R. E., Wolter, A., Stocke, J. T., Morris, S. L., & Henry, J. P. 1990, ApJS, 72, 567
Kollgaard, R. I., Wardle, J. F. C., Roberts, D. H., & Gabuzda, D. C. 1992, AJ, 104, 1687
Kühr, H., Witzel, A., Pauliny-Toth, I. I. K., & Nauber, U. 1981, A&AS, 45, 367
Laing, R. A. 1988, Nature, 331, 149
Lind, K. R., & Blandford, R. D. 1985, ApJ, 295, 358
Maccacaro, T., Gioia, I. M., Wolter, A., Zamorani, G., & Stocke, J. T. 1988, ApJ, 326, 680
Maraschi, L., Celotti, A., & Ghisellini, G. 1991, in The Physics of Active Galactic Nuclei, ed. W. J. Duschl & S. J. Wagner (Berlin: Springer), 605
Maraschi, L., Ghisellini, G., & Celotti, A. 1992, ApJ, 397, L5
Maraschi, L., Ghisellini, G., Tanzi, E., & Treves, A. 1986, ApJ, 310, 325
Marshall, H. L. 1985, ApJ, 299, 109
Morganti, R., Fosbury, R. A. E., Hook, R. N., Robinson, A., & Tsvetanov, Z. 1992, MNRAS, 256, 1P
Morris, S. L., Stocke, J. T., Gioia, I. M., Schild, R. E., Wolter, A., Maccacaro, T., & Della Ceca, R. 1991, ApJ, 380, 49
Padovani, P. 1992, A&A, 256, 399
Padovani, P., & Urry, C. M. 1990, ApJ, 356, 75
———. 1992, ApJ, 387, 449
Stickel, M., Padovani, P., Urry, C. M., Fried, J. W., & Kuhr, H. 1991, ApJ, 374, 431
Stocke, J. T., Morris, S. L., Gioia, I. M., Maccacaro, T., Schild, R. E., Wolter, A., Fleming, T. A., & Henry, J. P. 1991, ApJS, 76, 813
Treves, A., et al. 1989, ApJ, 341, 733
Ulrich, M.-H. 1989, in BL Lac Objects, ed. L. Maraschi, T. Maccacaro, & M.-H. Ulrich (Berlin: Springer), 45
Urry, C. M., Maraschi, L., & Phinney, S. E. 1991a, Comm. Ap., 15, 111
Urry, C. M., Marziani, P., & Calvani, M. 1991b, ApJ, 371, 510
Urry, C. M., & Padovani, P. 1991, ApJ, 371, 60
Urry, C. M., Padovani, P., & Stickel, M. 1991c, ApJ, 382, 501
Urry, C. M., & Shafer, R. A. 1984, ApJ, 280, 569
Wall, J. V., & Peacock, J. A. 1985, MNRAS, 216, 173
Wardle, J. F. C., Moore, R. L., & Angel, J. R. P. 1984, ApJ, 279, 93
Worrall, D. M., & Wilkes, B. J. 1990, ApJ, 360, 396
Zensus, T. 1989, in BL Lac Objects, ed. L. Maraschi, T. Maccacaro, & M.-H. Ulrich (Berlin: Springer), 3